

Article

A General Framework for Material Properties Calculation and the Free Vibration Analysis of New Three-Phase Composite Cylindrical Shell Structures

Wei Zhang ^{1,2} , Jinqiu Duan ¹, Tao Liu ^{1,*} , Yan Zheng ³ and Yingjing Qian ¹

¹ Beijing Key Laboratory of Nonlinear Vibrations and Strength of Mechanical Structures, Beijing University of Technology, Beijing 100124, China; sandyzhang9@163.com (W.Z.); duanjinqiu@emails.bjut.edu.cn (J.D.); qianyjingjing@bjut.edu.cn (Y.Q.)

² School of Civil Engineering and Architecture, Guangxi University, Nanning 530004, China

³ Department of Mathematics, Beijing Institute of Graphic Communication, Beijing 102600, China; zhengyan@bigc.edu.cn

* Correspondence: liu_tao@bjut.edu.cn

Abstract: New three-phase composite structures reinforced synergistically by nano-fillers and macroscopic fibers have great application potential. This paper presents a general framework for material properties calculation and the free vibration analysis of three-phase composite shell structures. Based on this methodological system, the free vibration characteristics of three types of nano-enhanced functionally graded three-phase composite cylindrical shells are investigated. First, the equivalent mechanical properties of these three three-phase composites were evaluated using the Halpin–Tsai and Mori–Tanaka models. The governing equations for the cylindrical shells were derived based on the first-order shear deformation theory (FSDT) and Hamilton’s principle. The equations were discretized using Galerkin’s method and solved to obtain the natural frequencies and mode shapes. The finite element simulation results and existing literature verified the accuracy and reliability of the method in this paper. The synergistic effects of nano-reinforced fillers and macroscopic fibers on the free vibrations of these structures were also analyzed. Among them, the natural frequency of the three-phase composite cylindrical shells was the highest when graphene platelets (GPLs) were used as the nano-reinforced fillers, which was 150.32% higher than that of fiber-reinforced epoxy composite cylindrical shells. These studies provide theoretical guidance for the design and manufacture of such symmetric or antisymmetric structures in the future.

Keywords: three-phase composites; material characteristics; free vibrations; cylindrical shell



Citation: Zhang, W.; Duan, J.; Liu, T.; Zheng, Y.; Qian, Y. A General Framework for Material Properties Calculation and the Free Vibration Analysis of New Three-Phase Composite Cylindrical Shell Structures. *Symmetry* **2024**, *16*, 20. <https://doi.org/10.3390/sym16010020>

Academic Editors: Guangdong Tian, Yong Peng, Zhiwu Li, Amir M. Fathollahi-Fard and Honghao Zhang

Received: 1 November 2023

Revised: 16 December 2023

Accepted: 18 December 2023

Published: 22 December 2023



Copyright: © 2023 by the authors. Licensee MDPI, Basel, Switzerland. This article is an open access article distributed under the terms and conditions of the Creative Commons Attribution (CC BY) license (<https://creativecommons.org/licenses/by/4.0/>).

1. Introduction

Composite materials have been called the shape of aerospace’s future. With the increasing application of composite materials in the aerospace industry, certain limitations have been exposed [1], the most troublesome of which is their inability to withstand damage from lightning strikes [2]. The new three-phase composite materials reinforced synergistically by nano-fillers and carbon fibers offer substantial benefits in dealing with this conundrum [3,4]. In recent years, there has been a growing surge in research focusing on the vibration characteristics of three-phase composite structures [5]. However, most existing studies are fragmented, and there is an urgent need to develop a systematic and general framework for the material properties calculation and vibration analysis of new three-phase composite structures. A general framework could facilitate more effective and coordinated efforts in this research field for the vibrations of three-phase composite structures. In this paper, we take the new functionally graded (FG) three-phase composite cylindrical shell as an example and attempt to solve some fundamental problems, including the calculation of equivalent material parameters for three-phase composite materials,

the establishment of a free vibration analysis model for three-phase composite structures, and the solution of natural frequencies and mode shapes.

As we all know, the composite structure has excellent mechanical properties, and it is widely used in aerospace, automotive, and defense fields [6]. The continuous fiber-reinforced composite structure is one of the most common components in engineering. To meet the material performance requirements of some special types of equipment and reduce the problem of stress concentration in composite laminated materials, the concept of FG composite materials has been proposed [7]. In recent years, researchers have incorporated nano-reinforced fillers into the matrix according to a certain FG distribution to constitute FG nano-reinforced composite materials. Nano-reinforced fillers, such as carbon nanotubes (CNTs), graphene platelets (GPLs), and their derivatives, with excellent mechanical properties, are ideal reinforcements for the preparation of high-performance FG nano-reinforced composite materials. However, the production of CNTs and GPLs is difficult and expensive. There is a need to find some relatively affordable and easy-to-manufacture graphene derivatives as an alternative. Graphene oxide platelets (GOPLs), the derivative of graphene, are relatively easier and cheaper to manufacture as they are the base materials for synthesizing graphene. Recently, related research on composite structures has been a hot spot for structure vibration [8]. For the vibrations of the FG composite panel and shell structures reinforced by CNTs or GPLs, there are several valuable studies [9], but research on the vibrations of GOPL-reinforced composite structures is very limited.

Recently, the concept of three-phase composite materials has been proposed to further improve the mechanical properties of two-phase composite materials. Firstly, the nano-reinforced fillers are mixed with the matrix to form a hybrid matrix (HM), then the macro-level fiber reinforcement is used to strengthen the HM to form a three-phase composite material [10]. Compared to traditional two-phase composites, three-phase composite materials have superior mechanical properties and richer comprehensive performance. It is of great significance to reduce the weight of composite structures and improve the vibration characteristics of these structures.

Several researchers have published some reports on the mechanical properties of three-phase composite materials, but there are fewer reports on the vibrations of three-phase composite structures, which are mainly focused on three-phase composite structures with CNTs as the nano-reinforced fillers [11]. Ebrahimi et al. [12,13] calculated the effective material properties of three-phase composite material, including the polymer, carbon fibers, and CNTs, using the Halpin–Tsai model and analyzed the vibration characteristics of these plates. Rezaiee-Pajand et al. Yousefi et al. [14] investigated the free vibrations of a three-phase composite-truncated conical shell, in which the three-phase composite material consisted of a polymer, CNTs, and carbon fibers, and the effective elastic properties were calculated based on the Mori–Tanaka–Eshelby method and the Han homogenization method. Sobhani et al. [15] calculated the equivalent mechanical properties of three-phase composites composed of a carbon fiber/graphene/polymer matrix using the Halpin–Tsai method and Mori–Tanaka scheme. Maleki et al. [16] investigated the free vibration characteristics of three-phase composite conical shells. Nopour et al. [17] investigated the vibration characteristics of three-phase composite thin-walled shell structures. By contrast, the vibration characteristics of the three-phase composite structures associated with GPLs or GOPLs receive much less attention, even though the cost of mass production of graphene and its derivatives is much lower than that of CNTs [18–20]. At present, the comparison study between the free vibration characteristics of the FG three-phase composite cylindrical shell with CNTs, GOPLs, and GPLs has not yet been reported. Therefore, there is an urgent need to develop a systematic and general framework for the material properties calculation and vibration analysis of new three-phase composite structures.

In this paper, we propose a general framework to solve vibration fundamental problems for the material properties calculation and vibration analysis of three-phase composite structures, as shown in Figure 1. We take new FG three-phase composite cylindrical shells as an example to analyze their vibration characteristics. First, the material properties of

three-phase composites are calculated using the Halpin–Tsai and Mori–Tanaka models and the mixing rule. Then, the governing equations of the structures are given based on the FSDT and the Hamilton principle. The Galerkin method is used to discretize the governing equations, and the natural frequencies and mode shapes are obtained by solving the characteristic equations. The accuracy and reliability of the computational method are verified by comparing the results with the existing literature and finite elements. Finally, the effects of different parameters on the natural frequency of three-phase composite structures are investigated.

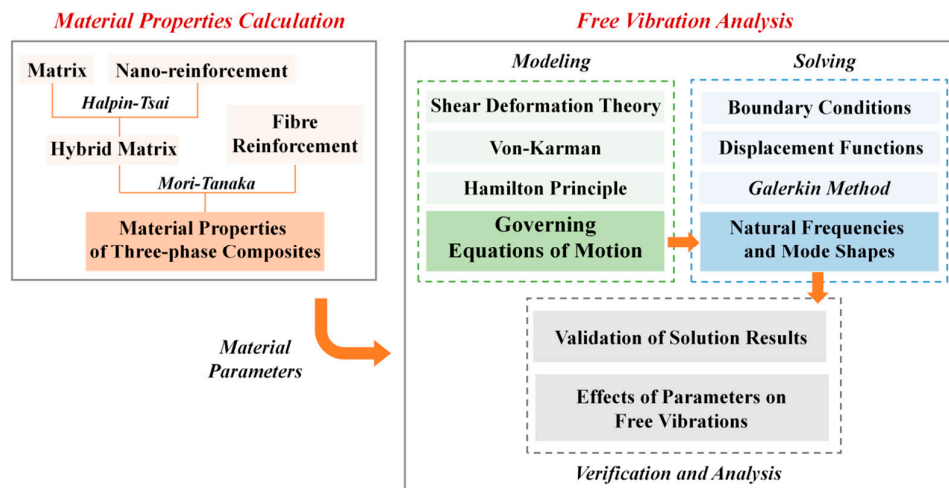


Figure 1. A schematic diagram of the computational procedure for material properties and free vibrations of the three-phase composite structure is given.

2. Determination of Material Properties

In this paper, epoxy resin is used as the polymer matrix with single-walled carbon nanotubes (SWCNTs), graphene oxide platelets (GOPLs), and graphene platelets (GPLs) as the three kinds of nano-reinforced fillers, and carbon fibers were selected for the macro and reinforcement. The material property parameters of these materials are detailed in Tables 1–3. It should be mentioned that all material characteristics are taken from the literature. In this paper, a general framework for determining the equivalent material properties of three-phase composites is given, as shown in Figure 1. The equivalent material properties of the nanofiller-reinforced epoxy matrix were first determined using the Halpin–Tsai method. Then, carbon fiber-reinforced HM forms a three-phase composite, and the Mori–Tanaka model is used to determine the equivalent material properties of the three-phase composite. Finally, the mixing law was used to determine the equivalent density and the equivalent Poisson’s ratio.

Table 1. The material properties of epoxy polymer, SWCNT [21,22], GPL [15], and GOPL [23,24] are given.

Material	E_e (GPa)	ν_e	ρ_e (kg/m ³)
8551-7 epoxy polymer (matrix)	4.08	0.38	1272
Single-walled carbon nanotube (SWCNT)	640	0.33	1350
Graphene platelets (GPL)	1010	0.186	1062.5
Graphene oxide platelet (GOPL)	444.8	0.165	1090

Table 2. The geometrical properties of SWCNT [21,22], GPL [15], and GOPL [23,24] are given.

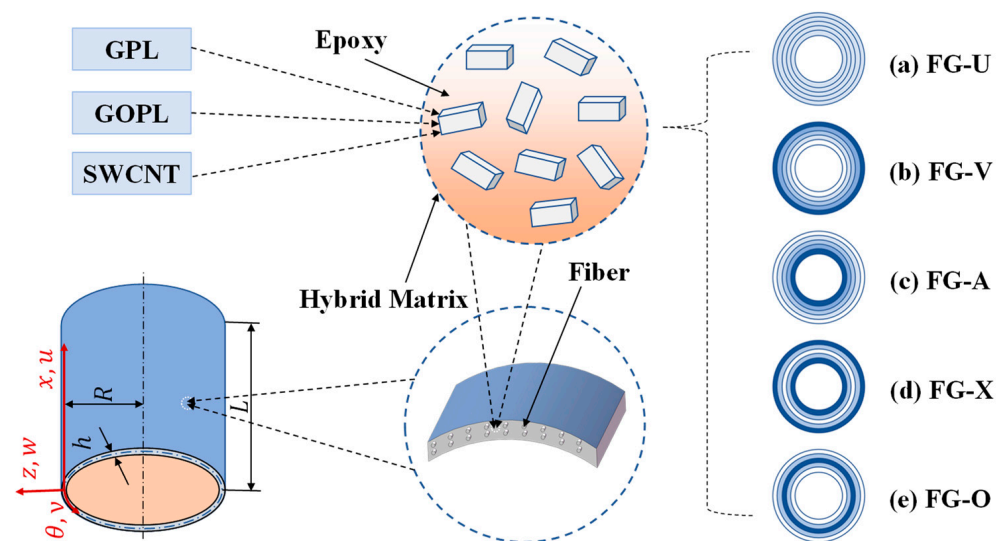
Material	$d_{\text{SWCNT}}(\mu\text{m})$	$L_{\text{SWCNT}}(\mu\text{m})$	$t_{\text{SWCNT}}(\mu\text{m})$
Single-walled carbon nanotube (SWCNT)	1.40	25.00	0.34
Material	$L_{\text{GPL}}(\mu\text{m})$	$W_{\text{GPL}}(\mu\text{m})$	$h_{\text{GPL}}(\mu\text{m})$
Graphene platelets (GPLs)	2.5	1.5	1.5
Material	$d_{\text{GOPL}}(\text{nm})$	$t_{\text{GOPL}}(\text{nm})$	
Graphene oxide platelet (GOPL)	500	0.95	

Table 3. The material properties of IM-7 carbon fiber [15,25] are given.

Material	$E_f^1(\text{Gpa})$	$E_f^2(\text{Gpa})$	ν_f^{12}	ν_f^{13}	$G_f^{12}(\text{Gpa})$	$G_f^{23}(\text{Gpa})$	$\rho_f(\text{kg/m}^3)$
Carbon fiber	276.0	19.0	0.2	0.2	27.0	7.0	1780.0

2.1. Material Properties of Hybrid Matrix

In this paper, the different nano-reinforced fillers are distributed in the epoxy resin matrix in FG forms, which constitute three kinds of different HMs. We considered five kinds of FG forms, including FG-U, FG-V, FG-A, FG-X, and FG-O. The distributions of nano-reinforced fillers in the direction of the shell thickness under the form of different FG forms are shown in Figure 2, where the darker color indicates higher contents.

**Figure 2.** The model and coordinate system of functionally graded three-phase composite cylindrical shells reinforced synergistically with nano-reinforced fillers and macroscopic fibers are given.

The equations for calculating the volume fraction of nano-reinforced fillers in each layer under different FG forms [15] are shown as follows:

$$\begin{aligned}
 \text{FG-U} : V_N(Z) &= V_N^0, & \text{FG-V} : V_N(Z) &= V_N^0 \left(1 + \frac{2Z}{h}\right), \\
 \text{FG-A} : V_N(Z) &= V_N^0 \left(1 - \frac{2Z}{h}\right), & \text{FG-X} : V_N(Z) &= V_N^0 \left(4 \frac{|Z|}{h}\right), \\
 \text{FG-O} : V_{\text{GPL}}(Z) &= 2V_{\text{GPL}}^0 \left(1 - \frac{2|Z|}{h}\right).
 \end{aligned} \quad (1)$$

In Equation (1), $V_N(Z)$ denotes the volume fraction of each layer of nano-reinforced fillers along the thickness direction. h and Z denote the total thickness and the coordinate values in the thickness direction, respectively. V_N^0 denotes the volume fraction of total

nano-reinforced fillers to the total epoxy resin, which is related to the mass fraction and density of the nano-reinforced fillers as well as the density of the substrate, as shown in the following equation:

$$V_N^0 = \frac{W_N^0}{W_N^0 + \rho_N(1 - W_N^0)/\rho_e}. \quad (2)$$

In Equation (2), ρ_e denotes the density of the epoxy matrix. W_N^0 and ρ_N denote the mass fraction and density of the nano-reinforced filler, respectively.

The formulas for calculating the equivalent material properties of SWCNTs or GPL-reinforced epoxy resin composites can be found in references [15,21], which are not introduced in detail due to space limitations. This paper only lists the calculation process for the equivalent material properties of the HM composed of the GOPL-reinforced epoxy resin. The specific parameters are listed in Tables 1 and 2 [21–24]. Halpin–Tsai micromechanics is a semi-empirical method that enables the properties of composites to be expressed in terms of the material properties of the matrix and reinforcing phases, as well as their occupancy and geometry [23]. The equivalent elastic modulus of the HM is calculated using the Halpin–Tsai micromechanics rule [24,26], as shown in the following equation:

$$E_{HM} = 0.49 \times \frac{1 + \xi_1 \eta_1 V_N(Z)}{1 - \eta_1 V_N(Z)} \times E_e + 0.51 \times \frac{1 + \xi_2 \eta_2 V_N(Z)}{1 - \eta_2 V_N(Z)} \times E_e. \quad (3)$$

where Young's modulus of the HM is denoted as E_{HM} , and Young's modulus of the epoxy resin is denoted as E_e . The parameters η_1 , η_2 , ξ_1 and ξ_2 can be expressed by the following equations:

$$\eta_1 = \frac{(E_{GOPL}/E_e) - 1}{(E_{GOPL}/E_e) + \xi_1}, \eta_2 = \frac{(E_{GOPL}/E_e) - 1}{(E_{GOPL}/E_e) + \xi_2}, \xi_1 = \xi_2 = \frac{2d_{GOPL}}{t_{GOPL}}. \quad (4)$$

In the above equations, the elastic modulus of GOPL is denoted as E_{GOPL} , and the geometry of GOPL is denoted by d_{GOPL} and t_{GOPL} . Poisson's ratio and the density of the HM consisting of each layer of the GOPL-reinforced epoxy can be calculated from the mixing rule as follows:

$$v_{HM}(Z) = v_{GOPL}V_N(Z) + v_eV_e(Z), \rho_{HM}(Z) = \rho_{GOPL}V_N(Z) + \rho_eV_e(Z). \quad (5)$$

where v_{GOPL} and ρ_{GOPL} denote Poisson's ratio and density, respectively.

Then, we obtained the variation in elastic modulus along the thickness direction of the HM composed of SWCNTs, GOPLs, and GPL-reinforced epoxy resins under these five kinds of FG forms, respectively, as shown in Figure 3. We found that the trend of the elastic modulus of the HM along the thickness direction was consistent with three kinds of nano-reinforced fillers. Taking the HM composed of the GPL-reinforced epoxy resin as an example, Young's modulus does not change with the change in the thickness direction coordinate in the FG-U form because the GPLs are uniformly distributed in the epoxy resin matrix. Young's modulus under the FG-V form increases significantly with the thickness direction coordinate because the mass fraction of GPLs under the FG-V form increases closer to the top layer of the shell, which leads to a gradual increase in the stiffness from the bottom to the top layer of the HM. The FG-A form is the opposite of the FG-V form. Young's modulus under the FG-X form increases and then decreases with the coordinates in the thickness direction. The reason for this is that the mass fraction of GPLs under the FG-X form is largest at the top and bottom layers of the shell and smallest at the mid-plane layer of the shell. This leads to a decrease and then an increase in the stiffness value when going from the bottom layer to the mid-plane layer and then to the top layer. The FG-O form as opposed to the FG-X form. However, Young's modulus of the HM reinforced by GPLs is the largest at various FG forms, Young's modulus of the HM reinforced by GOPLs is second, and Young's modulus of the HM reinforced by SWCNTs is the smallest.

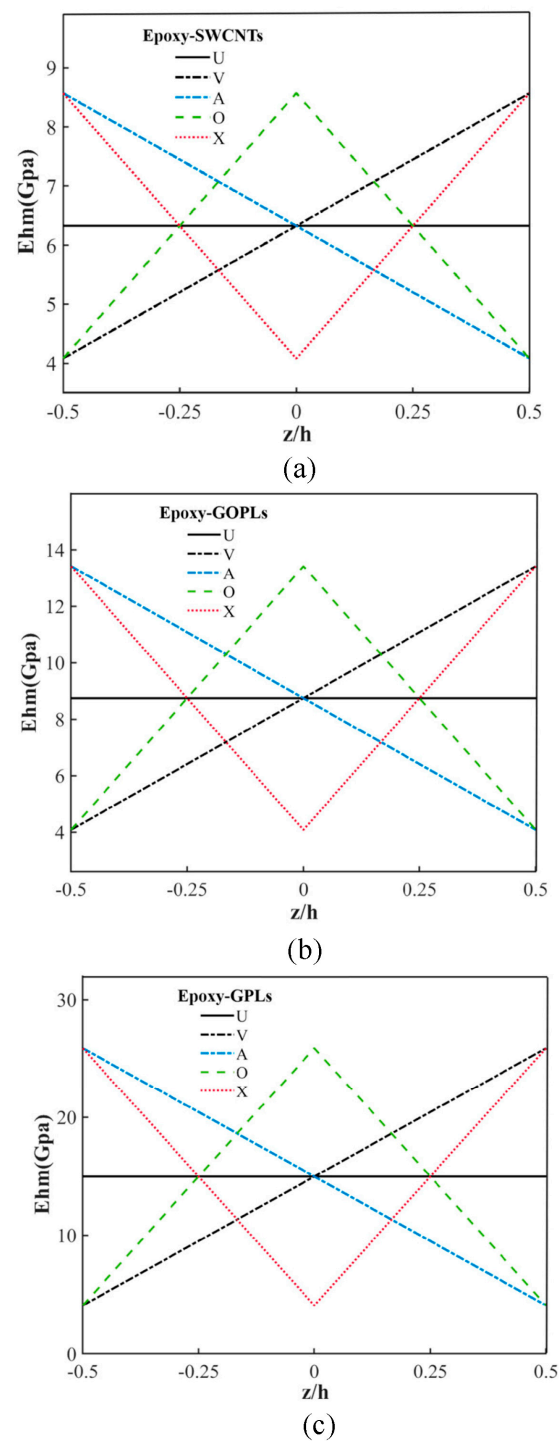


Figure 3. The changes in the equivalent elastic modulus of the hybrid matrix along the thickness direction corresponding to different distribution forms are given. (a) Epoxy-SWCNTs' functional gradient composites. (b) Epoxy-GOPLs' functional gradient composites. (c) Epoxy-GPLs' functional gradient composites.

2.2. Material Properties of Three-Phase Composites

In the previous subsection, the equivalent material properties of the three kinds of HM in each layer were calculated, respectively. The addition of macroscopic carbon fiber reinforcement into the HM can constitute a three-phase composite material, and the equivalent material properties of this three-phase composite material are calculated in this subsection according to the Mori-Tanaka method, where the Mori-Tanaka method is

expressed using the average behavior of the matrix and fiber materials. The longitudinal modulus and transverse modulus of elasticity of the carbon fiber are defined as E_f^1 and E_f^2 , the in-plane shear modulus and external shear modulus are denoted as G_f^{12} and G_f^{13} , Poisson's ratio is denoted as ν_f^{12} , and density is denoted as ρ_f , respectively. The carbon fiber reinforcement is considered to be transversely isotropic with the properties of $\nu_f^{12} = \nu_f^{13}$ and $E_f^2 = E_f^3$. The material property parameters of carbon fiber are detailed in Table 3 [15,26]. The Mori–Tanaka method proposes a scheme based on an elastic homogenization method using the average behavior of the matrix and fiber materials [15]. The specific equations for calculating the equivalent material properties of three-phase composite materials composed of the carbon fibers and the hybrid matrix from the Mori–Tanaka method [15,27] are as follows:

$$E_{eff}^1 = V_f E_f^1 + (1 - V_f) E_{HM} + 2V_f (1 - V_f) Z_1 (\nu_f^{12} - \nu_{HM})^2, \quad (6)$$

$$E_{eff}^2 = \frac{E_{eff}^1 / (1 - (\nu_{HM})^2)}{\frac{1}{1 - (\nu_{HM})^2} + 2V_f \frac{E_{eff}^1}{Z_2} \left(1 + \nu_f^{23} - \frac{E_f^2}{E_{HM}} (1 + \nu_{HM})\right) + V_f Z_1 \frac{E_f^1}{E_{HM}} \left(\frac{1 + \nu_{HM}}{E_{HM}} - \frac{2}{E_f^1} + \frac{1 - \nu_f^{23}}{E_f^2}\right)}, \quad (7)$$

$$\nu_{eff}^{12} = \nu_{HM} + 2V_f \frac{Z_1}{E_{HM}} (\nu_f^{12} - \nu_{HM}) (1 - (\nu_{HM})^2), \quad (8)$$

$$G_{eff}^{12} = G_{eff}^{13} = \frac{E_{HM}}{2(1 - V_f)(1 + \nu_{HM})} \left\{ 1 + V_f - 4V_f \left[1 + V_f + 2(1 - V_f) \frac{G_f^{12}}{E_{HM}} (1 + \nu_{HM}) \right]^{-1} \right\}, \quad (9)$$

$$G_{eff}^{23} = \frac{E_{HM}}{2(1 + \nu_{HM}) + V_f \left(\frac{1 - V_f}{8 - 8(\nu_{HM})^2} + \frac{1}{\frac{E_{HM}}{G_f^{23}} - 2(1 + \nu_{HM})} \right)^{-1}}. \quad (10)$$

In Equations (6)–(10), E_{eff}^1 , E_{eff}^2 , ν_{eff}^{12} , G_{eff}^{12} and G_{eff}^{23} denote the longitudinal equivalent modulus of elasticity, the transverse equivalent modulus of elasticity, longitudinal Poisson's ratio, in-plane equivalent shear modulus, and out-of-plane equivalent shear modulus, respectively. V_f denotes the volume fraction of the carbon fibers. The expressions for Z_1 and Z_2 are shown as follows:

$$Z_1 = \left(-2(1 - V_f) \frac{(\nu_f^{12})^2}{E_f^1} + (1 - V_f) \frac{1 - \nu_f^{23}}{E_f^2} + \frac{(1 + \nu_{HM})(1 + V_f(1 - 2\nu_{HM}))}{E_{HM}} \right)^{-1}, \quad (11)$$

$$Z_2 = E_f^2 (3 + V_f - 4\nu_{HM}) (1 + \nu_{HM}) + (1 - \nu_f) E_{HM} (1 + \nu_f^{23}). \quad (12)$$

The equivalent density (ρ_{eff}) of three-phase composite materials composed of the carbon fibers and hybrid matrix can be calculated according to the mixing rule using the following equation:

$$\rho_{eff} = \rho_f V_f + \rho_{HM} V_{HM}. \quad (13)$$

Three-phase composite materials have more excellent material properties compared with traditional two-phase symmetric/antisymmetric laminated composite materials or FG composite materials. Figure 4 shows the equivalent material properties of four different composite materials with different volume fractions of carbon fiber. These four composite materials include carbon fiber-reinforced epoxy resin composite laminated material and three kinds of three-phase composite materials with SWCNTs, GOPLs, and GPLs as nano-reinforced fillers, respectively. Three-phase composite materials have a mass fraction of nano-reinforced fillers of 1%; the FG-U distribution in the epoxy resin matrix forms the HM, the antisymmetric layup angle of the carbon fibers is $[0_4^{\circ}/90_4^{\circ}/0_4^{\circ}/90_4^{\circ}]$, and the volume fraction is 0.10. Overall, the equivalent material properties of these four kinds of composite

materials are significantly increased with the increase in the volume fraction of the carbon fibers. Carbon fiber-reinforced epoxy-laminated composite materials have the smallest equivalent Young's modulus and equivalent shear modulus, followed by the three-phase composite materials with SWCNTs as nano-reinforced fillers, while the three-phase composite materials with GPLs as nano-reinforced fillers have the largest equivalent Young's modulus and equivalent shear modulus.

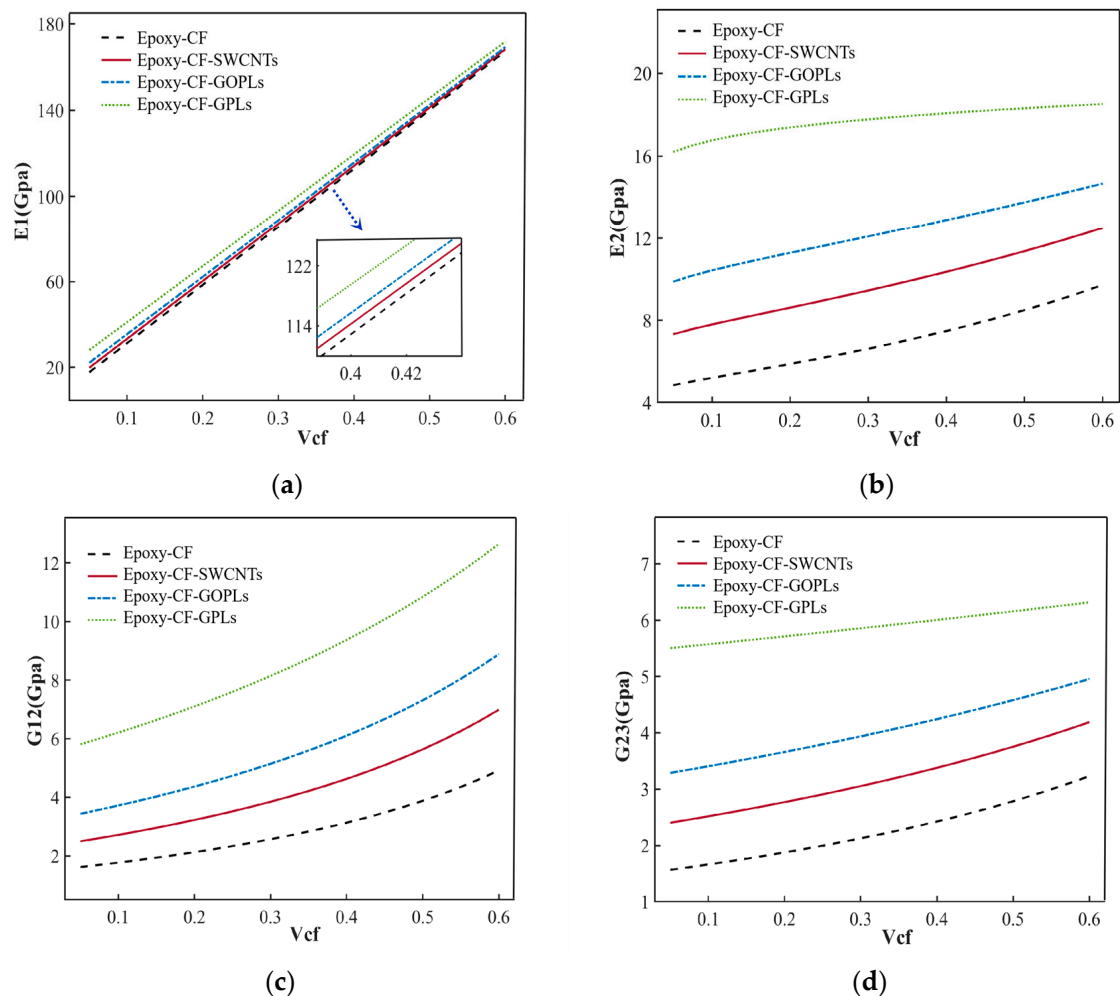


Figure 4. The change curves of equivalent material properties for three-phase composite materials with a carbon fiber volume fraction are shown. (a) Longitudinal elastic modulus (E1). (b) Transverse elastic modulus (E2). (c) In-plane shear modulus (G12). (d) Out-of-plane shear modulus (G23).

3. Governing Equations and Solution Procedure

The three-phase composite materials are made by adding nano-reinforced fillers to the traditional two-phase symmetric/antisymmetric-laminated composite materials. Compared with the traditional two-phase composite materials, the three-phase composite materials have higher stiffness and better comprehensive mechanical properties, which can be used to reduce the weight of the cylindrical shell structures as well as to improve their vibration characteristics. The model of three-phase composite cylindrical shells reinforced synergistically by nano-reinforced fillers and carbon fibers is shown in Figure 2. The column coordinate system is established in the mid-plane of the cylindrical shell, where x , θ and z denote the axial direction, circumferential direction, and radial direction of the cylindrical shell, respectively. u , v , and w denote the displacement of any point on the cylindrical shell in the axial, circumferential, and radial directions. The axial length, radius, and thickness of the cylindrical shell are denoted by L , R and h , respectively. If there is

no further specification, the geometrical parameters of the cylindrical shell are taken as $L = 2.00$ m, $R = 1.00$ m and $h = 0.05$ m.

Based on the first-order shear theory and Hamilton principle, The derivation of the governing equations for cylindrical shells refers to the classical literature [18,28].

The first-order shear deformation theory is shown as follows:

$$u(x, \theta, z, t) = u_0(x, \theta, t) + z\varphi_x(x, \theta, t), \quad (14)$$

$$v(x, \theta, z, t) = v_0(x, \theta, t) + z\varphi_\theta(x, \theta, t), \quad (15)$$

$$w(x, \theta, z, t) = w_0(x, \theta, t). \quad (16)$$

In Equations (14)–(16), u_0 , v_0 , and w_0 denote the displacements. Furthermore, φ_x denotes the mid-surface transverse rotation around the θ axis. φ_θ denotes the normal rotation of the mid-surface around the x axis. The Von Karman strain–displacement relationship is shown as follows:

$$\begin{Bmatrix} \varepsilon_{xx} \\ \varepsilon_{\theta\theta} \\ \gamma_{x\theta} \\ \gamma_{xz} \\ \gamma_{\theta z} \end{Bmatrix} = \begin{Bmatrix} \varepsilon_{xx}^0 \\ \varepsilon_{\theta\theta}^0 \\ \gamma_{x\theta}^0 \\ \gamma_{xz}^0 \\ \gamma_{\theta z}^0 \end{Bmatrix} + z \begin{Bmatrix} \varepsilon_{xx}^1 \\ \varepsilon_{\theta\theta}^1 \\ \gamma_{x\theta}^1 \\ \gamma_{xz}^1 \\ \gamma_{\theta z}^1 \end{Bmatrix}, \quad (17)$$

where

$$\begin{Bmatrix} \varepsilon_{xx}^0 \\ \varepsilon_{\theta\theta}^0 \\ \gamma_{x\theta}^0 \\ \gamma_{xz}^0 \\ \gamma_{\theta z}^0 \end{Bmatrix} = \begin{Bmatrix} \frac{\partial u_0}{\partial x} \\ \frac{\partial v_0}{R\partial\theta} + \frac{w_0}{R} \\ \frac{\partial u_0}{R\partial\theta} + \frac{\partial v_0}{\partial x} \\ \varphi_x + \frac{\partial w_0}{\partial x} \\ \varphi_\theta + \frac{\partial w_0}{R\partial\theta} - \frac{v_0}{R} \end{Bmatrix}, \quad \begin{Bmatrix} \varepsilon_{xx}^1 \\ \varepsilon_{\theta\theta}^1 \\ \gamma_{x\theta}^1 \\ \gamma_{xz}^1 \\ \gamma_{\theta z}^1 \end{Bmatrix} = \begin{Bmatrix} \frac{\partial \varphi_x}{\partial x} \\ \frac{\partial \varphi_\theta}{R\partial\theta} \\ \frac{\partial \varphi_x}{R\partial\theta} + \frac{\partial \varphi_\theta}{\partial x} \\ 0 \\ 0 \end{Bmatrix}. \quad (18)$$

In Equations (17) and (18), ε_{xx} and $\varepsilon_{\theta\theta}$ are the principal strains and $\gamma_{x\theta}$, γ_{xz} and $\gamma_{\theta z}$ are the tangential strains. The relationship of strains and stresses is expressed as follows:

$$\begin{Bmatrix} \sigma_{xx} \\ \sigma_{\theta\theta} \\ \tau_{x\theta} \\ \tau_{xz} \\ \tau_{\theta z} \end{Bmatrix}^k = \begin{bmatrix} \bar{Q}_{11} & \bar{Q}_{12} & & & \\ \bar{Q}_{12} & \bar{Q}_{22} & & & \\ & & \bar{Q}_{66} & & \\ & & & \bar{Q}_{44} & \\ & & & & \bar{Q}_{55} \end{bmatrix}^k \begin{Bmatrix} \varepsilon_{xx} \\ \varepsilon_{\theta\theta} \\ \gamma_{x\theta} \\ \gamma_{xz} \\ \gamma_{\theta z} \end{Bmatrix}, \quad (19)$$

In Equation (19), the number of located layers is denoted by k . The layup angle of the carbon fibers in each layer in the FG three-phase composite cylindrical shell is denoted by θ . And \bar{Q}_{ij} ($i, j = 1, 2, 3, 4, 5, 6$) denotes the conversion stiffness coefficient as follows:

$$\bar{Q}_{11} = Q_{11} \cos^4 \theta + 2(Q_{12} + 2Q_{66}) \sin^2 \theta \cos^2 \theta + Q_{22} \sin^4 \theta, \quad (20)$$

$$\bar{Q}_{12} = (Q_{11} + Q_{22} - 4Q_{66}) \sin^2 \theta \cos^2 \theta + Q_{12} (\sin^4 \theta + \cos^4 \theta), \quad (21)$$

$$\bar{Q}_{22} = Q_{11} \sin^4 \theta + 2(Q_{12} + 2Q_{66}) \sin^2 \theta \cos^2 \theta + Q_{22} \cos^4 \theta, \quad (22)$$

$$\bar{Q}_{16} = (Q_{11} - Q_{12} - 2Q_{66}) \sin \theta \cos^3 \theta + (Q_{12} - Q_{22} + 2Q_{66}) \cos \theta \sin^3 \theta, \quad (23)$$

$$\bar{Q}_{26} = (Q_{11} - Q_{12} - 2Q_{66}) \cos \theta \sin^3 \theta + (Q_{12} - Q_{22} + 2Q_{66}) \sin \theta \cos^3 \theta, \quad (24)$$

$$\bar{Q}_{66} = (Q_{11} + Q_{22} - 2Q_{12} - 2Q_{66}) \sin^2 \theta \cos^2 \theta + Q_{66} (\sin^4 \theta + \cos^4 \theta), \quad (25)$$

$$\bar{Q}_{44} = Q_{55} \sin^2 \theta + Q_{44} \cos^2 \theta, \quad (26)$$

$$\bar{Q}_{55} = Q_{44} \sin^2 \theta + Q_{55} \cos^2 \theta. \quad (27)$$

where

$$Q_{11} = \frac{E_{eff}^1}{1 - \nu_{eff}^{12}\nu_{eff}^{21}}, Q_{12} = \frac{\nu_{eff}^{12}E_{eff}^2}{1 - \nu_{eff}^{12}\nu_{eff}^{21}}, Q_{22} = \frac{E_{eff}^2}{1 - \nu_{eff}^{12}\nu_{eff}^{21}}, \quad (28)$$

$$Q_{44} = G_{eff}^{23}, Q_{55} = G_{eff}^{13}, Q_{66} = G_{eff}^{12}. \quad (29)$$

The equations for the membrane stress and membrane moment are shown as follows:

$$\begin{Bmatrix} N_{xx} \\ N_{\theta\theta} \\ N_{x\theta} \end{Bmatrix} = \begin{Bmatrix} A_{11} & A_{12} & A_{16} \\ A_{12} & A_{22} & A_{26} \\ A_{16} & A_{26} & A_{66} \end{Bmatrix} \begin{Bmatrix} \varepsilon_{xx}^0 \\ \varepsilon_{\theta\theta}^0 \\ \gamma_{x\theta}^0 \end{Bmatrix} + \begin{Bmatrix} B_{11} & B_{12} & B_{16} \\ B_{12} & B_{22} & B_{26} \\ B_{16} & B_{26} & B_{66} \end{Bmatrix} \begin{Bmatrix} \varepsilon_{xx}^1 \\ \varepsilon_{\theta\theta}^1 \\ \gamma_{x\theta}^1 \end{Bmatrix}, \quad (30)$$

$$\begin{Bmatrix} M_{xx} \\ M_{\theta\theta} \\ M_{x\theta} \end{Bmatrix} = \begin{Bmatrix} B_{11} & B_{12} & B_{16} \\ B_{12} & B_{22} & B_{26} \\ B_{16} & B_{26} & B_{66} \end{Bmatrix} \begin{Bmatrix} \varepsilon_{xx}^0 \\ \varepsilon_{\theta\theta}^0 \\ \gamma_{x\theta}^0 \end{Bmatrix} + \begin{Bmatrix} D_{11} & D_{12} & D_{16} \\ D_{12} & D_{22} & D_{26} \\ D_{16} & D_{26} & D_{66} \end{Bmatrix} \begin{Bmatrix} \varepsilon_{xx}^1 \\ \varepsilon_{\theta\theta}^1 \\ \gamma_{x\theta}^1 \end{Bmatrix}, \quad (31)$$

$$\begin{Bmatrix} Q_\theta \\ Q_x \end{Bmatrix} = K \begin{Bmatrix} A_{44} & A_{45} \\ A_{45} & A_{55} \end{Bmatrix} \begin{Bmatrix} \gamma_{\theta z}^0 \\ \gamma_{x\theta}^0 \end{Bmatrix}. \quad (32)$$

In the above equations, the shear correction factor $K = \frac{5}{6}$. A_{ij} , B_{ij} , D_{ij} and I_i ($i = 0, 1, 2$) denotes the extensional stiffness, extensional-bending stiffness, bending stiffness, and mass moment of inertia, respectively, as shown in the following equations:

$$(A_{ij}, B_{ij}, D_{ij}) = \int_{-\frac{h}{2}}^{\frac{h}{2}} \bar{Q}_{ij}(1, z, z^2) dz = \sum_{k=1}^N \int_{z_k}^{z_{k+1}} \bar{Q}_{ij}^k(1, z, z^2) dz, \quad (33)$$

$$I_i = \int_{-\frac{h}{2}}^{\frac{h}{2}} z^i \rho_{eff} dz \quad (i = 0, 1, 2). \quad (34)$$

In Equations (33) and (34), h denotes the total thickness of the shell, N denotes the total number of layers in the shell, $[\bar{Q}_{ij}]^{(k)}$ denotes the stiffness term of the k layer, and z denotes the coordinate value along the thickness direction.

The extended Hamilton principle can be expressed as follows:

$$\int_{t_2}^{t_1} (\delta T - \delta U + \delta W) dt = 0, \quad (35)$$

In Equation (35), δU , δT and δW denote the virtual strain energy, the virtual kinetic energy, and the virtual potential energy performed by the external force of the system, respectively. In this paper, no external force is involved in the study of the free vibration characteristics of the cylindrical shell, so δW is 0. The specific expressions for δU , δT and δW are shown as follows:

$$\delta T = \int_V \rho (\dot{u}\delta\dot{u} + \dot{v}\delta\dot{v} + \dot{w}\delta\dot{w}) dV, \quad (36)$$

$$\delta U = \int_V (\sigma_{xx}\delta\varepsilon_{xx} + \sigma_{\theta\theta}\delta\varepsilon_{\theta\theta} + \sigma_{x\theta}\delta\varepsilon_{x\theta} + \sigma_{xz}\delta\varepsilon_{xz} + \sigma_{\theta z}\delta\varepsilon_{\theta z}) dV, \quad (37)$$

$$\delta W = 0. \quad (38)$$

Substituting Equations (36)–(38) into Equation (35) yields the governing equations of the cylindrical shell as follows:

$$\delta u_0 : N_{xx,x} + \frac{N_{x\theta,\theta}}{R} = I_0\ddot{u}_0 + I_1\ddot{\varphi}_x, \quad (39)$$

$$\delta v_0 : N_{x\theta,x} + \frac{N_{\theta\theta,\theta}}{R} + \frac{Q_\theta}{R} = I_0\ddot{v}_0 + I_1\ddot{\varphi}_\theta, \quad (40)$$

$$\delta w_0 : -\frac{N_{\theta\theta}}{R} + Q_{x,x} + \frac{Q_{\theta,\theta}}{R} = I_0 \ddot{w}_0, \quad (41)$$

$$\delta \phi_x : M_{xx,x} + \frac{M_{x\theta,\theta}}{R} - Q_x = I_1 \ddot{u}_0 + I_2 \ddot{\phi}_x, \quad (42)$$

$$\delta \phi_\theta : M_{x\theta,x} + \frac{M_{\theta\theta,\theta}}{R} - Q_\theta = I_1 \ddot{v}_0 + I_2 \ddot{\phi}_\theta. \quad (43)$$

Then, we introduce the derivation of the solving procedure for solving the free vibrations of the FG three-phase composite cylindrical shell. Membrane stresses and bending moments at the boundary of the cylindrical shell are denoted by N and Q , respectively. N_{xx} and $N_{x\theta}$ denote the membrane stresses along the x -axis and the membrane stresses along the θ -axis, respectively. Q_x denotes the membrane stresses along the z -axis. M_{xx} and $M_{x\theta}$ denote the bending moments for the torsion around the θ -axis and the bending moments for the torsion around the x -axis, respectively. The constraint equations for the FG three-phase composite cylindrical shell with free boundary conditions at both ends are shown as follows:

At $x = 0$:

$$N_{xx} = N_{x\theta} = Q_x = 0, M_{xx} = M_{x\theta} = 0, \quad (44)$$

At $x = L$:

$$N_{xx} = N_{x\theta} = Q_x = 0, M_{xx} = M_{x\theta} = 0. \quad (45)$$

The assumption of the displacement function of the FG three-phase composite cylindrical shell is made using the modified Fourier cosine series method [29]. This method takes the form of a superposition of the Fourier cosine series, and the complementary functions are shown as follows:

$$u(x, \theta, t) = U(x, \theta)e^{i\omega t} = \left[\sum_{m=0}^M \sum_{n=0}^N U_{mn} \cos \lambda_m x \cos(n\theta) + \sum_{l=1}^2 \sum_{n=0}^N a_{1n} \zeta_l(x) \cos(n\theta) \right] e^{i\omega t}, \quad (46)$$

$$v(x, \theta, t) = V(x, \theta)e^{i\omega t} = \left[\sum_{m=0}^M \sum_{n=0}^N V_{mn} \cos \lambda_m x \sin(n\theta) + \sum_{l=1}^2 \sum_{n=0}^N b_{1n} \zeta_l(x) \sin(n\theta) \right] e^{i\omega t}, \quad (47)$$

$$w(x, \theta, t) = W(x, \theta)e^{i\omega t} = \left[\sum_{m=0}^M \sum_{n=0}^N W_{mn} \cos \lambda_m x \cos(n\theta) + \sum_{l=1}^2 \sum_{n=0}^N c_{1n} \zeta_l(x) \cos(n\theta) \right] e^{i\omega t}, \quad (48)$$

$$\phi_x(x, \theta, t) = \psi_x(x, \theta)e^{i\omega t} = \left[\sum_{m=0}^M \sum_{n=0}^N \psi_{xmn} \cos \lambda_m x \cos(n\theta) + \sum_{l=1}^2 \sum_{n=0}^N d_{1n} \zeta_l(x) \cos(n\theta) \right] e^{i\omega t}, \quad (49)$$

$$\phi_\theta(x, \theta, t) = \psi_\theta(x, \theta)e^{i\omega t} = \left[\sum_{m=0}^M \sum_{n=0}^N \psi_{\theta mn} \cos \lambda_m x \sin(n\theta) + \sum_{l=1}^2 \sum_{n=0}^N e_{1n} \zeta_l(x) \sin(n\theta) \right] e^{i\omega t}. \quad (50)$$

In Equations (46)–(50), M and N denote the number of truncation terms, both of which are non-negative integers. $\lambda_m = m\pi/L$, where m denotes the number of axial waves, n denotes the number of circumferential waves, and ω denotes the circular frequency of the FG three-phase composite cylindrical shell. U_{mn} , V_{mn} , W_{mn} , ψ_{xmn} and $\psi_{\theta mn}$ are generalized coordinates and also Fourier expansion coefficients. a_{1n} , b_{1n} , c_{1n} , d_{1n} , and e_{1n} are the coefficients of the corresponding augmentation functions, which can determine the type of boundary conditions. It must be ensured that the above coefficients can be derived. The complementary function is denoted by $\zeta_l(x)$ ($l = 1, 2$), and the complementary function is to eliminate the discontinuities of the displacement function and its derivatives, as well as to enhance the convergence of the expansion series. Based on the first-order shear deformation theory, the displacement function needs to be at least twice differentiable and continuous, so the augmentation function should be assumed as a third-degree polynomial. In this paper, the selected additive function is shown as follows:

$$\zeta_1(x) = x \left(\frac{x}{L} - 1 \right)^2, \zeta_2(x) = \frac{x^2}{L} \left(\frac{x}{L} - 1 \right). \quad (51)$$

The boundary condition equations represent the relationship between the two-dimensional generalized coordinates $U_{mn}, V_{mn}, W_{mn}, \psi_{xmn}, \psi_{\theta mn}$ and the complementary function coefficients $a_{ln}, b_{ln}, c_{ln}, d_{ln}, e_{ln}$ ($l = 1, 2$). Since the number of complementary function coefficients is the same as that of the boundary equation, complementary function coefficients can be expressed in two-dimensional generalized coordinates, which can be written in the form of the following matrix:

$$\mathbf{Y} = \mathbf{P}\mathbf{X}, \quad (52)$$

Here, \mathbf{P} is the coefficient matrix,

$$\mathbf{Y} = \{ a_0, \dots, a_n, b_0, \dots, b_n, c_0, \dots, c_n, d_0, \dots, d_n, e_0, \dots, e_n \}^T, \quad (53)$$

$$\mathbf{X} = \{ \mathbf{u}^T, \mathbf{v}^T, \mathbf{w}^T, \boldsymbol{\varphi}_x^T, \boldsymbol{\varphi}_\theta^T \}^T, \quad (54)$$

The control equations of motion are obtained by substituting Equations (46)–(50) and (51) into Equations (39)–(43). There are a total number of Fourier cosine coefficients, and the control equations are truncated using the Galerkin method. The truncated algebraic equations are expressed in the matrix form as follows:

$$\mathbf{S}\mathbf{X} + \mathbf{Q}\mathbf{Y} + \mathbf{F}\mathbf{X} + \mathbf{G}\mathbf{Y} = \mathbf{0}. \quad (55)$$

where \mathbf{S} , \mathbf{Q} , \mathbf{F} , and \mathbf{G} are coefficient matrices. Substituting Equation (52) into Equation (55) yields the following:

$$(\mathbf{M} + \mathbf{K})\mathbf{X} = \mathbf{0}, \quad (56)$$

where

$$\mathbf{M} = \mathbf{S} + \mathbf{P}\mathbf{Q}, \mathbf{K} = \mathbf{F} + \mathbf{P}\mathbf{G}. \quad (57)$$

Equation (56) is the standard characteristic equation, and the relevant numerical solutions for the natural frequencies and mode shapes of the FG three-phase composite cylindrical shell can be obtained by solving the eigenvalues and eigenvectors of this characteristic equation.

4. Method Verification

This section focuses on verifying the convergence and accuracy of the computational method in this paper. We investigate the law of the natural frequencies as the cylindrical shell converges gradually with the increase in the truncation number M and N , and we also verify the convergence of the natural frequency of FG composite cylindrical shells with the increase in the total number of layers. Then, the accuracy of the calculation method for the vibrations of the cylindrical shell is verified by comparing the results of this paper with the finite elements and the reference [30]. Moreover, the comparisons of the free vibrations of FG three-phase composite cylindrical shells with the finite element results are conducted, which further verifies the reliability of the computational method for calculating the free vibrations of FG three-phase composite cylindrical shells.

Firstly, the law of gradual convergence of the natural frequencies of the cylindrical shell with the increase in the truncation number is investigated. The geometrical parameters of the cylindrical shell are $L = 0.502$ m, $R = 0.0635$ m, and $h = 0.00163$ m. The material property parameters are $\rho = 7800$ kg/m³, $\mu = 0.28$ and $E = 2.1\text{E} + 11$ N. We considered the free boundary conditions at both ends. The comparison of the calculated results of the natural frequencies of the cylindrical shell with the finite element results for different truncation numbers (M, N) is shown in Table 4. We found that the natural frequencies of the cylindrical shell appeared to increase and gradually converge with the gradual increase in the number of cutoffs. When the truncation number was taken as $M = 14$ and $N = 14$, the difference between the natural frequencies of the cylindrical shell calculated by this method and the finite element calculation result was not more than 3.02%. It verified that the calculation method in this paper has good convergence and good accuracy with the increase in truncation number.

Table 4. The comparison and errors of the calculated results of the natural frequencies of the cylindrical shell with the finite element results for different truncation numbers given. ($L = 0.502$ m; $R = 0.0635$ m; $h = 0.00163$ m; $\rho_0 = 7800$ kg/m³; $\nu = 0.28$; $E = 2.1E + 11$ N/m²).

n	Present					Abaqus	Error
	M = 6 N = 6	M = 8 N = 8	M = 10 N = 10	M = 12 N = 12	M = 14 N = 14		
1	241.69	257.63	264.51	268.28	268.40	269.71	0.49%
2	267.45	267.85	268.11	268.37	270.90	277.03	2.21%
3	732.87	746.17	752.73	756.70	757.68	765.24	0.99%
4	735.20	749.97	754.79	756.97	760.75	774.68	1.80%
5	805.23	846.54	879.88	900.95	913.82	942.32	3.02%
6	959.65	984.99	1000.04	1008.62	1013.57	1020.10	0.64%

Secondly, the relationship between the rate of change in the natural frequencies and the number of layers of the FG cylindrical shell structure is investigated. The geometrical parameters of the FG cylindrical shell used for this study were $L = 2.00$ m, $R = 1.00$ m, and $h = 0.05$ m. The free boundary conditions at both ends were considered. Epoxy resin was selected as the matrix, GPLs were the nano-reinforced fillers, and the mass fraction of GPLs was 1.00%. The GPLs were distributed in the epoxy resin collectively in the FG-X form. The natural frequencies of the FG cylindrical shell were calculated when the total number of layers was 8, 10, 12, 14, 16, and 18, respectively. The rates of change in natural frequencies versus the number of layers were obtained after data processing, as shown in Figure 5. We found that the rates of change in natural frequencies of FG GPL-reinforced composite cylindrical shells decreased significantly with the increase in the total number of layers. When the total number of layers was 16, the variations in the first six orders of natural frequencies were all below 0.41%. Therefore, we considered the total number of layers as 16 to meet the realistic substitution of continuous FG composite materials and for the natural frequencies to converge. In the following studies in this paper, the total number of layers of FG composite cylindrical shells is taken as 16 unless otherwise stated.

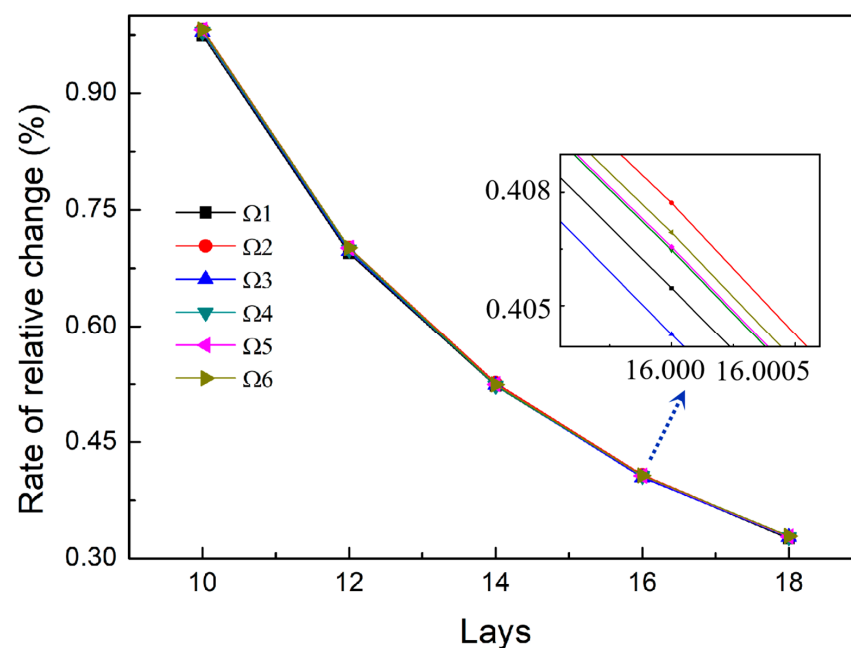
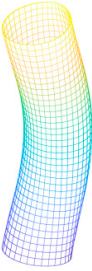
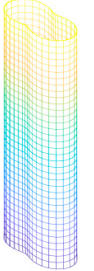
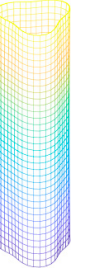
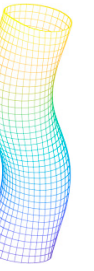
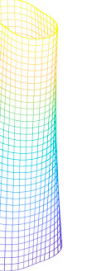
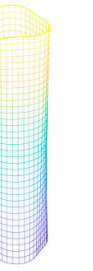
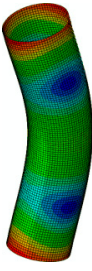
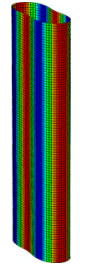
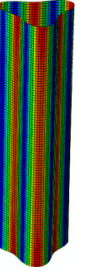
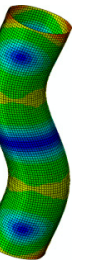
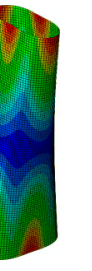
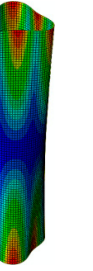


Figure 5. The rates of change for natural frequencies of functionally graded three-phase composite cylindrical shells with the number of layers are shown.

The accuracy of the calculation method of this paper is verified by comparing the results of this method with finite elements and the reference [30]. In Table 5, the natural frequencies and mode shapes of the cylindrical shells calculated in this paper are in good agreement with the finite element results and the results of the existing reference. The differences between the results of the cylindrical shell natural frequency calculations in this paper and those in the existing literature are not more than 0.35%. It is verified that the calculation method of this paper has good accuracy.

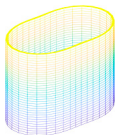
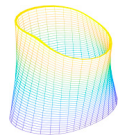
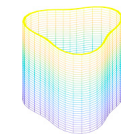
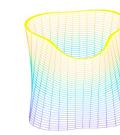
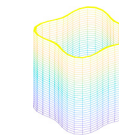
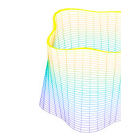
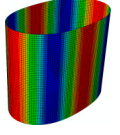
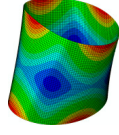
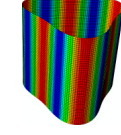
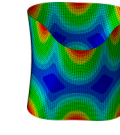
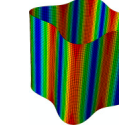
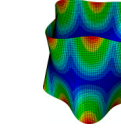
Table 5. Comparison of theoretical results on the natural frequencies and mode shapes of cylindrical shells under the free boundary conditions at both ends with finite element results and an existing reference is shown. ($L = 0.502$ m; $R = 0.0635$ m; $h = 0.00163$ m; $\rho_0 = 7800$ kg/m³; $\nu = 0.28$; $E = 2.1E + 11$ N/m²).

C-C	Mode No.					
	(m = 1, n = 1)	(m = 1, n = 2)	(m = 1, n = 3)	(m = 2, n = 1)	(m = 2, n = 2)	(m = 2, n = 3)
Present						
Abaqus						
Present	2479.31	268.49	758.30	4830.79	272.67	770.67
Abaqus	2481.30	269.71	765.24	4852.30	277.03	774.68
Dai [30]	2479.30	269.30	761.01	4840.40	276.51	770.66

Moreover, the natural frequencies and mode shapes of the FG three-phase composite cylindrical shells with SWCNTs as nano-reinforced fillers were investigated under the free boundary conditions at both ends and the calculation results were compared with the finite element results. The total mass fraction of SWCNTs was 1.00%, and the SWCNTs were distributed in the epoxy matrix to form the HM with the FG-X form. Carbon fibers were distributed in the antisymmetric form of $[0_4^{\circ}/90_4^{\circ}/0_4^{\circ}/90_4^{\circ}]$ layup angles in the HM, and the volume fraction of carbon fibers was 0.1. The geometrical parameters of the FG three-phase composite cylindrical shell were $L = 2.00$ m, $R = 1.00$ m, $h = 0.05$ m. The comparison of the calculation results of the natural frequencies and mode shapes of the FG three-phase composite cylindrical shell with the finite element (Abaqus) results is shown in Table 6. The first six orders of natural frequencies and mode shapes of the FG three-phase composite cylindrical shells are in good agreement with the finite element results. The differences between the calculation results and the finite element results for the natural frequencies of the cylindrical shell are not more than 1.10%, except for the second order of frequency. In particular, for the first-order natural frequency, the difference was 0.00% when two decimals were retained. Here, m denotes the number of axial half-waves, and n denotes the number of circumferential waves of the vibration modes of the cylindrical shell. Based on the calculation method in this paper, the mode shapes corresponding to the

first six orders of natural frequencies are the first-order ($m = 1, n = 2$), second-order ($m = 2, n = 2$), third-order ($m = 1, n = 3$), fourth-order ($m = 2, n = 3$), fifth-order ($m = 1, n = 4$), and sixth-order ($m = 2, n = 4$). The first six orders of natural frequencies and mode shapes of the FG three-phase composite cylindrical shells are in good agreement with the finite element results.

Table 6. Comparison of theoretical results on the natural frequencies and mode shapes of the functionally graded three-phase cylindrical shells with SWCNTs as nano-reinforced fillers under the free boundary conditions with finite element results is shown. ($L = 2$ m; $R = 1$ m; $h = 0.05$ m; FG-X; $W_{\text{SWCNT}} = 1\%$; $V_{\text{cf}} = 0.1$).

C-C	Mode No.					
	1	2	3	4	5	6
Present						
Abaqus						
Present	24.39	29.02	68.56	74.54	130.47	136.99
Abaqus	24.39	27.35	68.56	73.73	130.50	136.58
Error	0.00%	6.11%	0.00%	1.10%	0.02%	0.30%

5. Vibration Characteristics Analysis

In this section, we study the synergistic effects of macroscopic fiber reinforcements and nano-reinforcements on the natural frequencies of FG three-phase composite cylindrical shells. We chose three different nano-reinforced fillers, namely SWCNTs, GOPLs, and GPLs, and the carbon fiber was selected as the macroscopic-level fiber reinforcement. When studying the influential factor of nano-reinforcements, the effects of the type of nano-reinforced fillers, the content of nano-reinforced fillers, and the different FG forms on the natural frequencies of the FG three-phase composite cylindrical shells are mainly investigated. If the carbon fiber-related parameters are taken as variables, the effects of the content of carbon fibers and the layup angle on the natural frequencies of the FG three-phase composite cylindrical shells are studied. Without any special explanation, we considered the free boundary conditions at both ends, and the geometrical parameters were taken as $L = 2.00$ m, $R = 1.00$ m, and $h = 0.05$ m. The material property parameters of the epoxy resin matrix, nano-reinforced fillers, and carbon fiber are detailed in Tables 1–3.

5.1. Effects of Nano-Reinforced Fillers

Firstly, we studied the effects of different kinds of nano-reinforced fillers on the natural frequencies of the FG three-phase composite cylindrical shells. The nano-reinforced fillers are uniformly distributed in the epoxy resin reinforced by carbon fibers. In the subsequent calculations, the mass fraction of the nano-reinforced fillers was taken as 1.00%, if not otherwise specified. The antisymmetric layup angle of carbon fiber was $[0_4^{\circ}/90_4^{\circ}/0_4^{\circ}/90_4^{\circ}]$, and the content (V_{cf}) was 0.10. Four kinds of composite materials were selected as the independent variables, three kinds of which were the FG three-phase composite materials with SWCNTs, GOPLs, and GPLs as the nano-reinforced fillers, respectively, and one of which was the carbon fibers reinforced two-phase composite laminated material. The natural frequencies of cylindrical shells corresponding to these four kinds of composite materials are calculated. The results are shown in Figure 6.

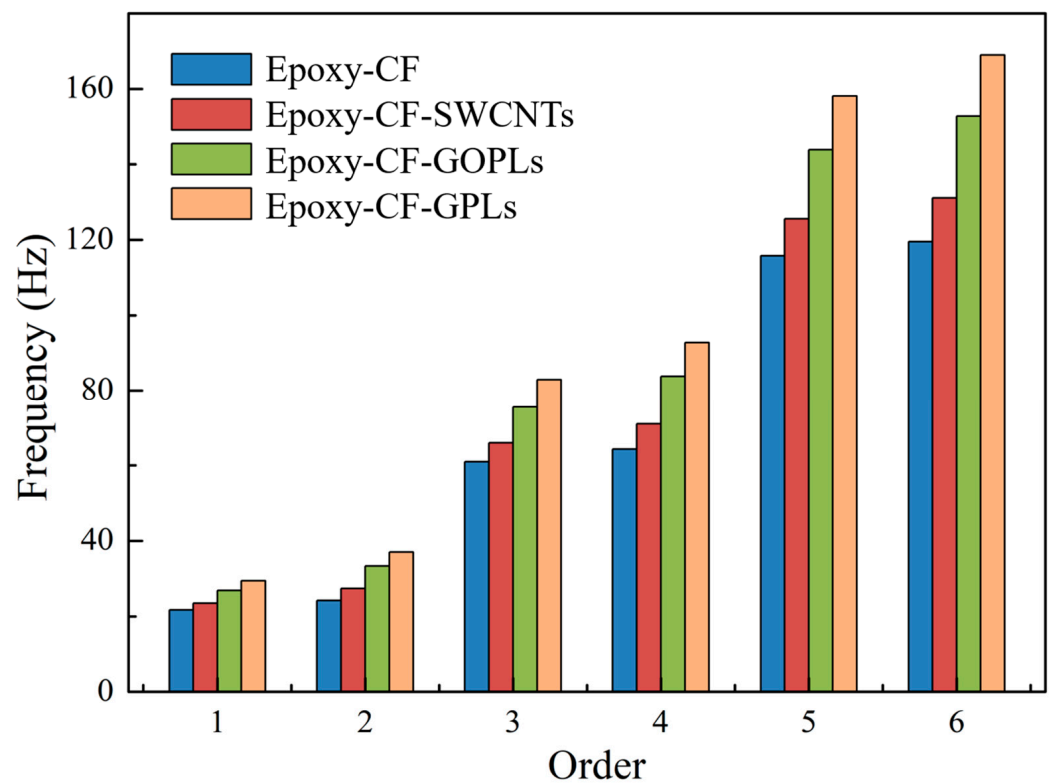


Figure 6. The natural frequencies of functionally graded three-phase composite cylindrical shells corresponding to different kinds of nano-reinforced fillers.

In Figure 6, it can be seen that carbon fibers reinforced with two-phase composite-laminated cylindrical shells had the smallest natural frequencies in the first six orders of vibrations, of which the first three orders are 21.70 Hz, 24.19 Hz, and 60.94 Hz, respectively. For the FG three-phase composite cylindrical shells, we found that the first six orders of natural frequencies of the cylindrical shells with GPLs as nano-reinforced fillers were relatively high, whereas the first three orders of natural frequencies were 29.43 Hz, 37.01 Hz, and 82.90 Hz, respectively; on the contrary, the first six orders of natural frequencies of the cylindrical shells with GOPLs as nano-reinforced fillers took second place, where the first three orders of natural frequencies were 23.46 Hz, 27.36 Hz, and 65.36 Hz, respectively. The first three orders of natural frequencies of the FG three-phase composite cylindrical shells with GPLs as nano-reinforcements were 35.62%, 53.00%, and 36.04% higher than those of carbon fiber-reinforced epoxy composite cylindrical shells, respectively. The reason for this phenomenon may be that the overall stiffness of the material increases, and the natural frequency of the cylindrical shell increases after the addition of nano-reinforced fillers to the carbon fiber-reinforced two-phase composite material.

Secondly, the effects of the content of nano-reinforced fillers on the natural frequencies of the FG three-phase composite cylindrical shells were investigated considering three kinds of nano-reinforced fillers, namely, SWCNTs, GOPLs, and GPLs, respectively. The nano-reinforced fillers were uniformly distributed into the epoxy resin reinforced by the carbon fibers. The mass fraction of nano-reinforced fillers took the range of 0.00–5.00%. The mass fraction of nano-reinforced fillers was used as the independent variable, and the natural frequencies of FG three-phase composite cylindrical shells were calculated corresponding to three kinds of nano-reinforced fillers, respectively. The relationship curves between the content of nano-reinforced fillers and the natural frequencies of the FG three-phase composite cylindrical shells with different nano-reinforced fillers are plotted in Figure 7.

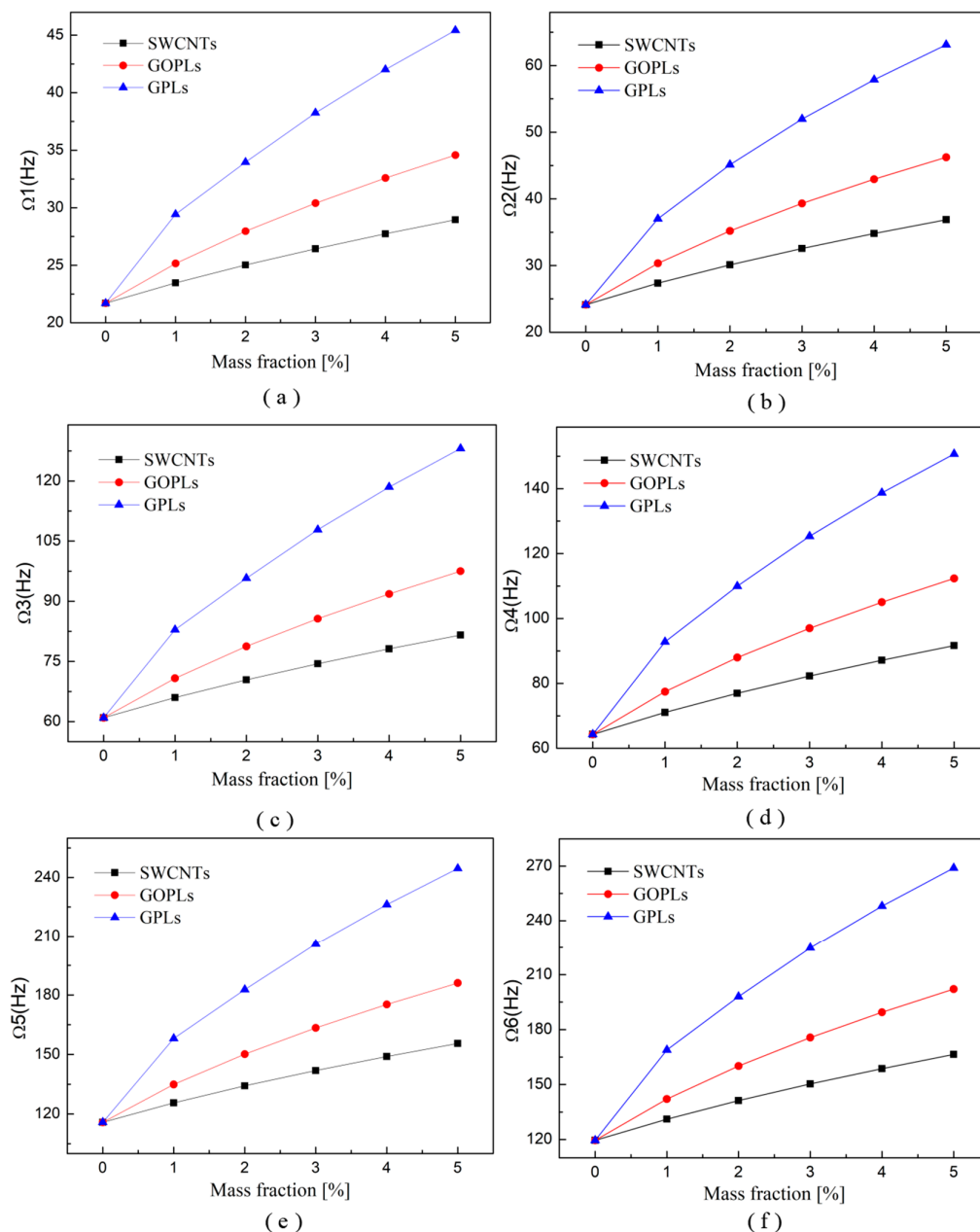


Figure 7. The change curves of natural frequencies of functionally graded three-phase composite cylindrical shells with the increase in the mass fraction of nano-reinforced fillers are shown. (a) First-order natural frequencies. (b) Second-order natural frequencies. (c) Third-order natural frequencies. (d) Fourth-order natural frequencies. (e) Fifth-order natural frequencies. (f) Sixth-order natural frequencies.

Figure 7a represents the curves of first-order natural frequencies versus the mass fraction of nano-reinforced fillers. The first-order natural frequencies of the FG three-phase composite cylindrical shells all increased significantly with the increase in the mass fraction of nano-reinforced fillers. Among them, the first-order natural frequency of FG three-phase composite cylindrical shells was relatively high when GPLs were used as the nano-reinforced fillers; GOPLs followed this, and minimum corresponded to SWCNTs. When the mass fraction of GPLs increased from 0.00% to 5.00%, the natural frequency of the FG three-phase composite cylindrical shell increased from 21.70 Hz to 45.43 Hz, an increase of 109.35%. When SWCNTs' mass fraction was increased from 0.00% to 5.00%, the natural frequency of the FG three-phase composite cylindrical shell increased from 21.70 Hz to

28.96 Hz, with an increase of 33.46%. It was found that, for the FG three-phase composite cylindrical shells, the first-order natural frequency at only 1.00% of GPLs was already higher than the natural frequency at 5.00% of SWCNTs. The first-order natural frequency of the FG three-phase composite cylindrical shell was 56.87% higher at 5.00% of GPLs than at 5.00% of SWCNTs. It can be seen that GPLs, as the nano-reinforced fillers, enhanced the composite materials much better than SWCNTs. In Figure 7b–f, we found that the rest of the five orders of natural frequencies followed a similar pattern. Overall, the first six orders of natural frequencies of the FG three-phase composite cylindrical shell increased significantly with the increase on the mass fraction of the nano-reinforced fillers, and each order natural frequency was relatively high when GPLs were used as the nano-reinforced fillers.

Finally, we also studied the influences of the FG forms of nano-reinforced fillers on the natural frequencies of the FG three-phase composite cylindrical shells. The volume fraction of carbon fibers was 0.10, and the antisymmetric layup angle was $[0_4^{\circ}/90_4^{\circ}/0_4^{\circ}/90_4^{\circ}]$. The mass fraction of nano-reinforced fillers was 1.00%. The FG form of nano-reinforced fillers was selected as the independent variable. We calculated the first six orders of natural frequencies of the FG three-phase composite cylindrical shells under the distribution of three kinds of nano-reinforced fillers in the form of FG-O, FG-V, FG-A, and FG-X, respectively. The column figures of the first six orders of natural frequencies of FG three-phase composite cylindrical shells with different FG forms under different nano-reinforced fillers are shown in Figure 8.

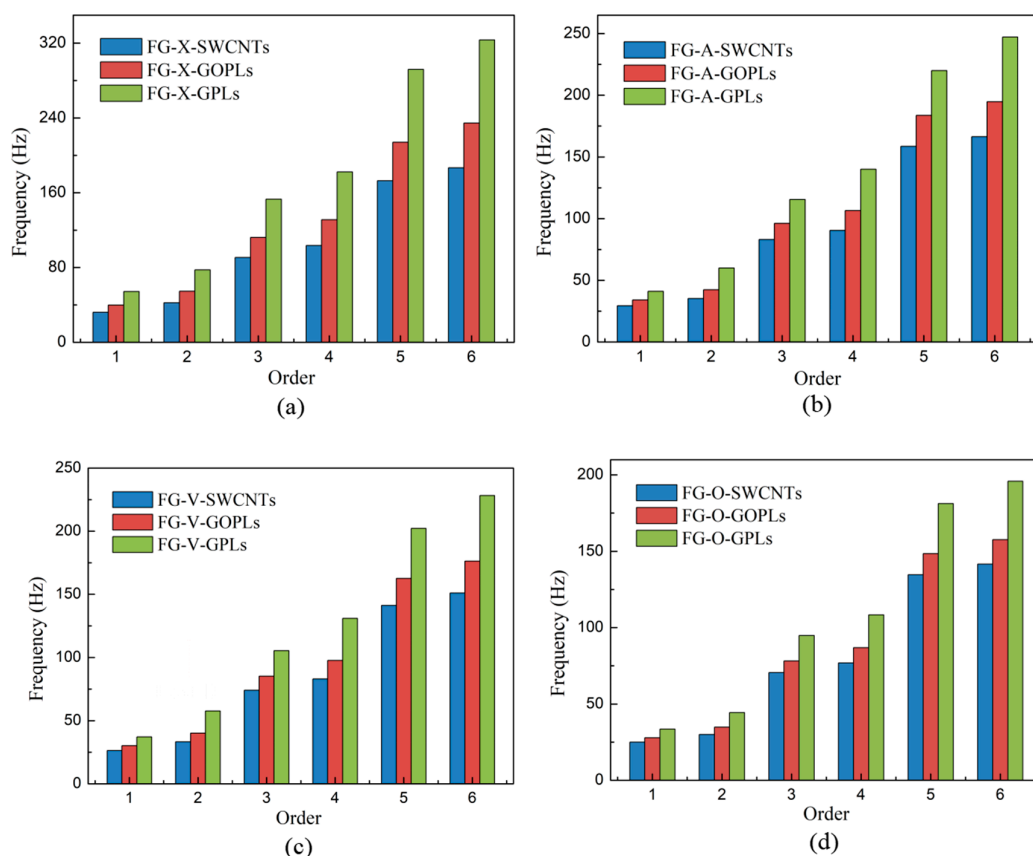


Figure 8. The natural frequencies of four kinds of FG three-phase composite cylindrical shells correspond to three kinds of nano-reinforced fillers. (a) FG-X three-phase composite cylindrical shells. (b) FG-A three-phase composite cylindrical shells. (c) FG-V three-phase composite cylindrical shells. (d) FG-O three-phase composite cylindrical shells.

Figure 8a represents the first six orders of natural frequencies for the FG three three-phase composite cylindrical shells under the FG-X form. The first six orders of natural frequencies of the three-phase composite cylindrical shells with GPLs as the nano-reinforced

fillers were higher, of which the first three orders of natural frequencies are 54.32 Hz, 77.45 Hz, and 153.06 Hz, respectively, and the first six orders of natural frequencies of FG three-phase composite cylindrical shells with GOPLs as the nano-reinforced fillers followed. When SWCNTs were used as the nano-reinforced fillers, the first six orders of natural frequencies of the FG three-phase composite cylindrical shells were low, while the first three orders of the natural frequencies were 32.20 Hz, 42.28 Hz, and 90.66 Hz, respectively. The first three orders of natural frequencies of the FG three-phase composite cylindrical shells with GPLs as the nano-reinforced fillers were higher than that of the FG three-phase composite cylindrical shells with SWCNTs of 68.70%, 83.18%, and 68.83%, respectively. A similar pattern was observed for the first six orders of natural frequencies of the FG three-phase composite cylindrical shells in the forms of FG-A, FG-V, and FG-O in Figure 8b–d. It was found that the natural frequencies of the FG three-phase composite cylindrical shells were highest when GPLs were used as nano-reinforced fillers for different FG forms.

5.2. Effects of Macroscopic Fiber Reinforcements

We studied the effect of the content of carbon fibers on the natural frequencies of FG three-phase composite cylindrical shells when SWCNTs, GOPLs, and GPLs were used as nano-reinforced fillers, respectively. The mass fraction of the nano-reinforced fillers was 1.00%, which was distributed in the form of FG-X in the epoxy resin matrix to form a hybrid matrix. The antisymmetric layup angle of carbon fibers was $[0_4^{\circ}/90_4^{\circ}/0_4^{\circ}/90_4^{\circ}]$, and the volume fraction of carbon fiber (Vcf) took the value range of 0.10–0.60 and was used as the independent variable. The natural frequencies of the FG three-phase composite cylindrical shells with different carbon fiber volume fractions were calculated for the three nano-reinforced fillers, SWCNTs, GOPLs, and GPLs, respectively. The curves of the carbon fiber volume fraction versus natural frequencies of the FG three-phase composite cylindrical shells with different nano-reinforced fillers are shown in Figure 9.

Figure 9a represents the relationship curves between the carbon fiber volume fraction (Vcf) and the first-order of natural frequencies. The first-order natural frequencies of the FG three-phase composite cylindrical shells all increased significantly with the increase in the carbon fiber volume fraction. The first-order natural frequencies of the FG three-phase composite cylindrical shells were relatively high when GPLs were used as the nano-reinforced fillers; the first order natural frequency of the FG three-phase composite cylindrical shell increased from 32.00 Hz to 45.23 Hz with an increase of 41.34%. If SWCNTs are selected as nano-reinforced fillers, the natural frequency of the FG three-phase composite cylindrical shell increases from 24.39 Hz to 43.04 Hz, which is an increase of 76.47%. It is interesting to note that the percentage increase in the first-order natural frequency of FG three-phase composite cylindrical shells with SWCNTs as nano-reinforced fillers is the largest, followed by GOPLs and GPLs are the smallest. In Figure 9b–f, we found that the remaining five orders of natural frequencies followed a similar pattern. Overall, the first six orders of the natural frequencies of the FG three three-phase composite cylindrical shells increased significantly with the increase in the volume fraction of carbon fiber. The natural frequencies of the FG three-phase composite cylindrical shells were relatively high when GPLs were used as nano-reinforced fillers.

Then, we also studied the effects of the carbon fiber symmetric/antisymmetric layup angle on the natural frequencies of the FG three-phase composite cylindrical shells. The natural frequencies of the FG three-phase composite cylindrical shells with different carbon fiber layup angles were calculated. In Figure 10, the histogram of each order of natural frequency of FG three-phase composite cylindrical shells with three different nano-reinforced fillers in the special carbon fiber layup angle is presented. We found that there were similar patterns, where FG three-phase composite cylindrical shells with GPLs as the nano-reinforced fillers had the highest first six orders of natural frequencies, followed by GOPLs. When SWCNTs were used as nano-reinforced fillers, the first six orders of the cylindrical shells had the smallest natural frequencies.

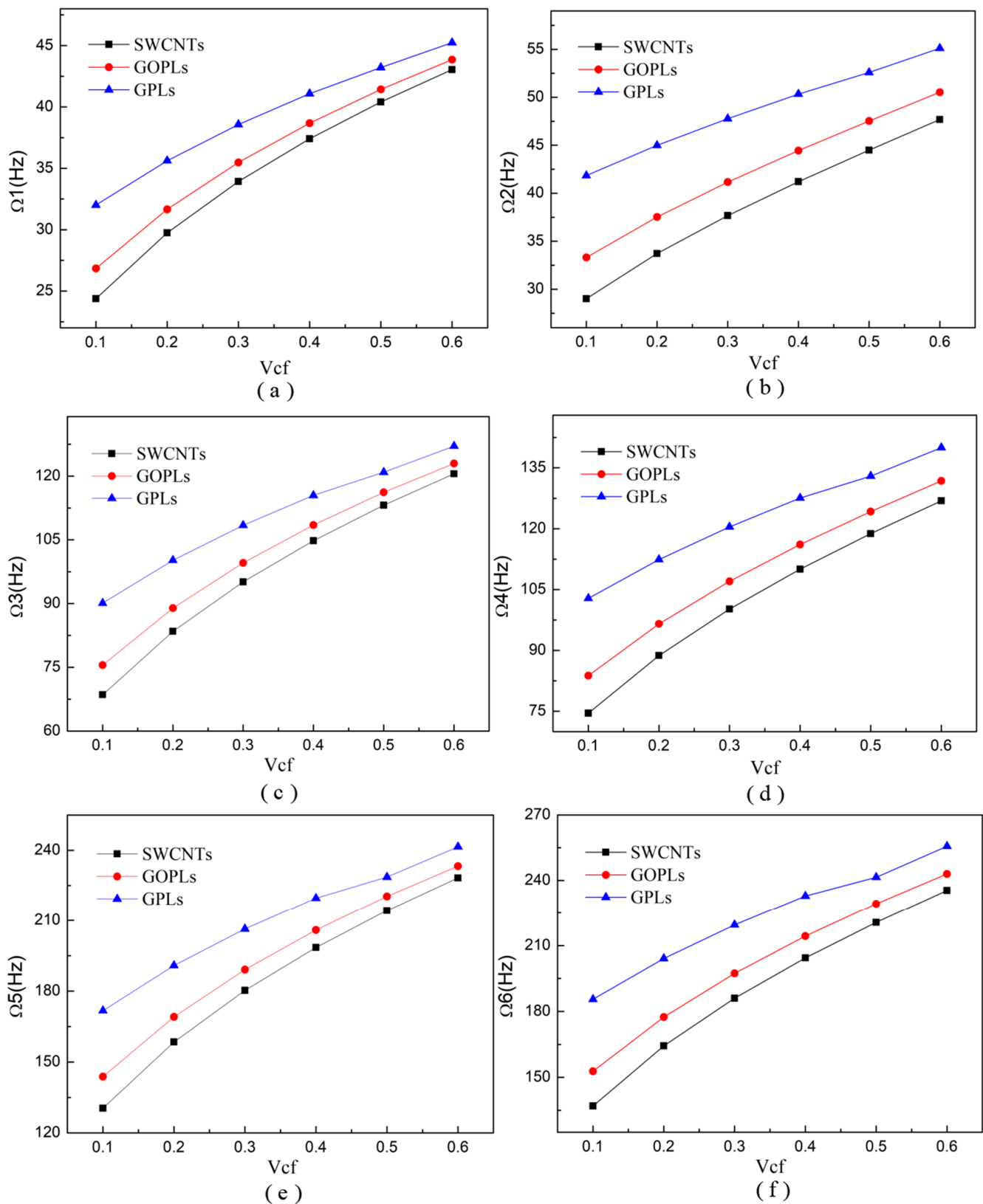


Figure 9. The change curves of natural frequencies of functionally graded three-phase composite cylindrical shells with increasing volume fractions of carbon fibers. (a) First-order natural frequencies. (b) Second-order natural frequencies. (c) Third-order natural frequencies. (d) Fourth-order natural frequencies. (e) Fifth-order natural frequencies. (f) Sixth-order natural frequencies.

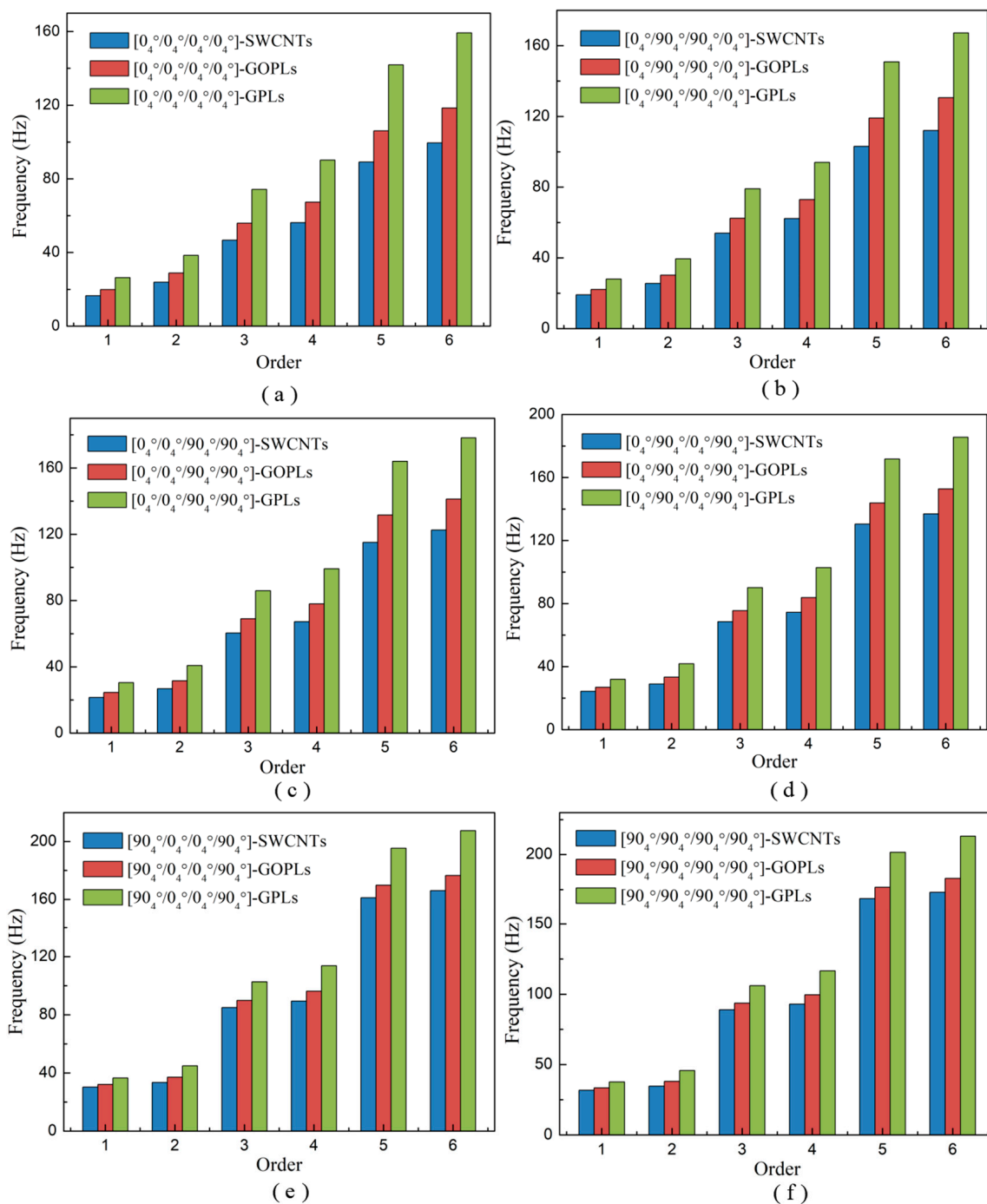


Figure 10. The natural frequencies of the functionally graded three-phase composite cylindrical shells with six kinds of carbon fiber layup angles are given corresponding to different nano-reinforced fillers. (a) The carbon fiber layup angle is $[0_4^\circ/0_4^\circ/0_4^\circ/0_4^\circ]$. (b) The carbon fiber layup angle is $[0_4^\circ/90_4^\circ/90_4^\circ/0_4^\circ]$. (c) The carbon fiber layup angle is $[0_4^\circ/0_4^\circ/90_4^\circ/90_4^\circ]$. (d) The carbon fiber layup angle is $[0_4^\circ/90_4^\circ/0_4^\circ/90_4^\circ]$. (e) The carbon fiber layup angle is $[90_4^\circ/0_4^\circ/0_4^\circ/90_4^\circ]$. (f) The carbon fiber layup angle is $[90_4^\circ/90_4^\circ/90_4^\circ/90_4^\circ]$.

6. Conclusions

This paper presents a general framework for the material properties calculation and free vibration analysis of new three-phase composite structures. Taking the FG three-phase composite cylindrical shell as an example, the corresponding research and conclusions demonstrate the feasibility of this general framework. In our research, the effects of different

types and contents of nano-reinforced fillers and the content of macroscopic fibers on the natural frequencies of the FG three-phase composite cylindrical shell are analyzed.

- (1) The synergistic enhancement effects of nano-reinforced fillers and macroscopic fibers were found, and the results of this paper show that the addition of nano-reinforced fillers is significant in improving the vibration characteristics of traditional two-phase composite structures.
- (2) It was found that the effects of the type, content, and FG form of nano-reinforced fillers on the free vibrations of the FG three-phase composite cylindrical shells are significant. A small number of nano-reinforced fillers in the carbon fiber-reinforced composite shell can significantly enhance its natural frequencies. Among them, a small amount (only 1%) of GPL acts as the nano-reinforced filler and, when added to the carbon fiber-reinforced composites in the form of FG-X, can increase the natural frequency of the composite cylindrical shell by 150.32%.
- (3) We also found that the content and layup angle of carbon fiber also had important influences on the natural frequencies of the FG three-phase composite cylindrical shells. With the increase in the carbon fiber volume fraction, the first six orders of natural frequencies of the FG three-phase composite cylindrical shells significantly increased.

The general framework proposed in this paper helps promote the solution of fundamental problems, including the calculation of equivalent material parameters and the free vibration analysis for the new three-phase composite structure, stimulating more effective research on its other vibration characteristics. This study also provides theoretical guidance for the design and manufacture of FG three-phase composite structures in aerospace, civil engineering, and rail transportation. The current methods used to find the vibration characteristics of three-phase composite shell structures show limitations under more complex loads or in complex environments such as those that are mild and wet. And we have not tried more numerical analysis methods. In the future, we aim to carry out research on the vibration characteristics of three-phase composite shell structures under more complex loads, mild humidity, and other complex environments, including natural vibration characteristics and nonlinear vibration characteristics. In addition, we will try more numerical methods, such as the differential quadrature method and the wavelet method.

Author Contributions: The contributions of all authors are given below. Conceptualization, T.L. and W.Z.; methodology, T.L. and J.D.; software, T.L. and J.D.; validation, J.D.; formal analysis, J.D.; investigation, T.L. and W.Z.; resources, W.Z.; data curation, J.D.; writing—original draft preparation, J.D.; writing—review and editing, T.L.; visualization, W.Z.; supervision, Y.Z., W.Z. and Y.Q.; project administration, T.L., W.Z. and Y.Q.; funding acquisition, T.L., Y.Z. and Y.Q. All authors have read and agreed to the published version of the manuscript.

Funding: The authors gratefully acknowledge the support of the National Natural Science Foundation of China (NNSFC) through Grant Nos. 12202018, 12332001, and 12322202, the Funding Projects of the Beijing Institute of Graphic Communication through Grant Nos. 20190123083 and 27170123038, the support of the China Postdoctoral Science Foundation through Grant Nos. 2021TQ0021 and 2022M710280, and the Funding Project for Postdoctoral Research from Beijing City and Chaoyang District.

Data Availability Statement: Data are contained within the article.

Conflicts of Interest: The authors declare no conflict of interest.

References

1. Shan, L.; Tan, C.Y.; Shen, X.; Ramesh, S.; Zarei, M.S.; Kolahchi, R.; Hajmohammad, M.H. The effects of nano-additives on the mechanical, impact, vibration, and buckling/post-buckling properties of composites: A review. *J. Mater. Res. Technol.* **2023**, *24*, 7570–7598. [[CrossRef](#)]
2. Gagné, M.; Therriault, D. Lightning strike protection of composites. *Prog. Aerosp. Sci.* **2014**, *64*, 1–16. [[CrossRef](#)]
3. Alemour, B.; Bradan, O.; Hassan, M.R. A Review of using conductive composite materials in solving lightening strike and ice accumulation problems in aviation. *J. Aerosp. Technol. Manag.* **2019**, *11*, e1919. [[CrossRef](#)]

4. Li, Y.; Zhang, H.; Huang, Z.; Bilotti, E.; Peijs, T. Graphite nanoplatelet modified epoxy resin for carbon fibre reinforced plastics with enhanced properties. *J. Nanomater.* **2017**, *2017*, 5194872. [[CrossRef](#)]
5. Rafiee, M.; Nitzsche, F.; Labrosse, M.R. Modeling and mechanical analysis of multiscale fiber-reinforced graphene composites: Nonlinear bending, thermal post-buckling and large amplitude vibration. *Int. J. Non-Linear Mech.* **2018**, *103*, 104–112. [[CrossRef](#)]
6. Cai, M.H.; Yang, T.; Li, H.W.; Yang, H.X.; Han, J.W. Experimental and simulation study on shielding performance of developed hydrogenous composites. *Space Sci. Technol.* **2022**, *2022*, 9754387. [[CrossRef](#)]
7. Tornabene, F. Free vibration analysis of functionally graded conical, cylindrical shell and annular plate structures with a four-parameter power-law distribution. *Comput. Methods Appl. Mech. Eng.* **2009**, *198*, 2911–2935. [[CrossRef](#)]
8. Liu, T.; Zhang, W.; Mao, J.J.; Zheng, Y. Nonlinear breathing vibrations of eccentric rotating composite laminated circular cylindrical shell subjected to temperature, rotating speed and external excitations. *Mech. Syst. Signal Process.* **2019**, *127*, 463–498. [[CrossRef](#)]
9. Zhang, L.W.; Song, Z.G.; Liew, K.M. Modeling aerothermoelastic properties and active flutter control of nanocomposite cylindrical shells in supersonic airflow under thermal environments. *Comput. Methods Appl. Mech. Eng.* **2017**, *325*, 416–433. [[CrossRef](#)]
10. Rezaiee-Pajand, M.; Sobhani, E.; Masoodi, A.R. Free vibration analysis of functionally graded hybrid matrix/fiber nanocomposite conical shells using multiscale method. *Aerosp. Sci. Technol.* **2020**, *105*, 105998. [[CrossRef](#)]
11. Karimiasl, M. Chaotic dynamics of a non-autonomous nonlinear system for a smart composite shell subjected to the hygro-thermal environment. *Microsyst. Technol.* **2019**, *25*, 2587–2607. [[CrossRef](#)]
12. Ebrahimi, F.; Habibi, S. Nonlinear eccentric low-velocity impact response of a polymer-carbon nanotube-fiber multiscale nanocomposite plate resting on elastic foundations in hygrothermal environments. *Mech. Adv. Mater. Struct.* **2018**, *25*, 425–438. [[CrossRef](#)]
13. Ebrahimi, F.; Dabbagh, A. Vibration analysis of multi-scale hybrid nanocomposite shells by considering nanofillers' aggregation. *Waves Random Complex Media* **2022**, *32*, 1060–1078. [[CrossRef](#)]
14. Yousefi, A.H.; Memarzadeh, P.; Afshari, H.; Hosseini, S.J. Agglomeration effects on free vibration characteristics of three-phase CNT/polymer/fiber laminated truncated conical shells. *Thin Walled Struct.* **2020**, *157*, 107077. [[CrossRef](#)]
15. Sobhani, E.; Masoodi, A.R. Natural frequency responses of hybrid polymer/carbon fiber/FG-GNP nanocomposites paraboloidal and hyperboloidal shells based on multiscale approaches. *Aerosp. Sci. Technol.* **2021**, *119*, 107111. [[CrossRef](#)]
16. Maleki, A.T.; Pourseifi, M.; Zakeri, M. Effect of agglomeration of the nanotubes on the vibration frequency of the multi-scale hybrid nanocomposite conical shells: A GDQ-based study. *Waves Random Complex Media* **2022**, *32*, 359–380. [[CrossRef](#)]
17. Nopour, R.; Ebrahimi, F.; Dabbagh, A.; Aghdam, M.M. Nonlinear forced vibrations of three-phase nanocomposite shells considering matrix rheological behavior and nano-fiber waviness. *Eng. Comput.* **2023**, *39*, 557–574. [[CrossRef](#)]
18. Amabili, M. Nonlinear vibrations of laminated circular cylindrical shells: Comparison of different shell theories. *Compos. Struct.* **2011**, *94*, 207–220. [[CrossRef](#)]
19. Liu, T.; Zheng, Y.; Qian, Y. Frequency change and mode shape transformation in free vibration analysis of three-phase composite thin plate under different boundary conditions. *J. Vib. Eng. Technol.* **2023**. [[CrossRef](#)]
20. Liu, T.; Duan, J.; Zheng, Y.; Qian, Y. Free vibrations of a new three-phase composite cylindrical shell. *Aerospace* **2023**, *10*, 1007. [[CrossRef](#)]
21. Kim, M.; Park, Y.-B.; Okoli, O.I.; Zhang, C. Processing, characterization, and modeling of carbon nanotube-reinforced multiscale composites. *Compos. Sci. Technol.* **2009**, *69*, 335–342. [[CrossRef](#)]
22. Arani, A.G.; Haghparast, E.; Zarei, H.B. Vibration of axially moving 3-phase CNTFPC plate resting on orthotropic foundation. *Struct. Eng. Mech.* **2016**, *57*, 105–126. [[CrossRef](#)]
23. Kasiri, R.; Massah, S.R. Mathematical modeling of concrete beams containing GO nanoparticles for vibration analysis and measuring their compressive strength using an experimental method. *Adv. Nano Res.* **2022**, *12*, 73–79.
24. Zhang, Z.; Li, Y.; Wu, H.; Zhang, H.; Wu, H.; Jiang, S.; Chai, G. Mechanical analysis of functionally graded graphene oxide-reinforced composite beams based on the first-order shear deformation theory. *Mech. Adv. Mater. Struct.* **2018**, *27*, 3–11. [[CrossRef](#)]
25. Sobhani, E.; Moradi-Dastjerdi, R.; Behdinan, K.; Masoodi, A.R.; Ahmadi-Pari, A.R. Multifunctional trace of various reinforcements on vibrations of three-phase nanocomposite combined hemispherical-cylindrical shells. *Compos. Struct.* **2022**, *279*, 101016. [[CrossRef](#)]
26. Arani, A.G.; Zarei, H.B.; Eskandari, M.; Pourmousa, P. Vibration behavior of visco-elastically coupled sandwich beams with magnetorheological core and three-phase carbon nanotubes/fiber/polymer composite facesheets subjected to external magnetic field. *J. Sandw. Struct. Mater.* **2019**, *21*, 2194–2218. [[CrossRef](#)]
27. Abaimov, S.G.; Khudyakova, A.A.; Lomov, S.V. On the closed form expression of the Mori-Tanaka theory prediction for the engineering constants of a unidirectional fiber-reinforced ply. *Compos. Sci. Technol.* **2016**, *142*, 1–6. [[CrossRef](#)]
28. Reddy, J.N. *Mechanics of Laminated Composite Plates and Shells: Theory and Analysis*; CRC Press: Boca Raton, FL, USA, 2004.
29. Zhang, W.; Fang, Z.; Yang, X.-D.; Liang, F. A series solution for free vibration of moderately thick cylindrical shell with general boundary conditions. *Eng. Struct.* **2018**, *165*, 422–440. [[CrossRef](#)]
30. Dai, L.; Yang, T.; Du, J.; Li, W.L.; Brennan, M.J. An exact series solution for the vibration analysis of cylindrical shells with arbitrary boundary conditions. *Appl. Acoust.* **2013**, *74*, 440–449. [[CrossRef](#)]

Disclaimer/Publisher's Note: The statements, opinions and data contained in all publications are solely those of the individual author(s) and contributor(s) and not of MDPI and/or the editor(s). MDPI and/or the editor(s) disclaim responsibility for any injury to people or property resulting from any ideas, methods, instructions or products referred to in the content.